Highlights

- Neural trajectories in the hippocampus exhibited greater variability during a working memory (WM) task compared to those in the entorhinal cortex and amygdala regions.

- The distance of neural trajectories between encoding and retrieval states in the hippocampus was memory-load dependent during a WM task.

- Hippocampal neural trajectories fluctuated between the encoding and retrieval states in a task-dependent manner during both baseline and sharp-wave ripple (SWR) periods.

- Hippocampal neural trajectories shifted from encoding to retrieval states during SWR period.

Hippocampal neural fluctuations during encoding and retrieval in a human working memory task: Encoding-to-retrieval shift during sharp-wave ripples

Yusuke Watanabe[a,*], Yuji Ikegaya[b,c,d], Takufumi Yanagisawa[a,e]

[a]*Institute for Advanced Cocreation studies, Osaka University, 2-2 Yamadaoka, Suita, 565-0871, Osaka, Japan*
[b]*Graduate School of Pharmaceutical Sciences, The University of Tokyo, 7-3-1 Hongo, Tokyo, 113-0033, Japan*
[c]*Institute for AI and Beyond, The University of Tokyo, 7-3-1 Hongo, Tokyo, 113-0033, Japan*
[d]*Center for Information and Neural Networks, National Institute of Information and Communications Technology, 1-4 Yamadaoka, Suita City, 565-0871, Osaka, Japan*
[e]*Department of Neurosurgery, Osaka University Graduate School of Medicine, 2-2 Yamadaoka, Osaka, 565-0871, Japan*

Abstract

Working memory (WM) is indispensable for numerous cognitive functions, although the underlying neural mechanisms have not been fully elucidated. While the hippocampus and sharp-wave ripple complexes (SWRs) – brief, synchronous neural events within the hippocampus – are acknowledged for their importance in memory consolidation and retrieval, their association with WM tasks remains unclear. The present study posits that hippocampal multiunit activity patterns, in concert with SWRs, manifest distinct dynamics during WM tasks. We analyzed a dataset comprising intracranial electroencephalogram recordings from the medial temporal lobe (MTL) of nine epilepsy patients engaged in an eight-second Sternberg task. Gaussian-process factor analysis was utilized to extract low-dimensional neural representations, or 'trajectories', within MTL regions during the WM task. Our results reveal that the hippocampus demonstrates the most significant fluctuation in neural trajectory relative to the entorhinal cortex and amygdala. Furthermore, trajectories' dissimilarity measured between encoding and retrieval phases is dependent on memory load. Notably, hippocampal trajectories fluctuate during the retrieval phase and exhibit task-dependent shifts between encoding and retrieval states, both during baseline and SWR events. This fluctuation transitions from encoding to retrieval states in the presence of SWRs. These findings reinforce the pivotal role of the hippocampus in WM tasks and suggest a new hypothesis: the hippocampus alters its functional state from encoding to retrieval during SWRs.

Keywords: working memory, WM, memory load, hippocampus, sharp-wave ripples, SWR, humans

1. Introduction

Working memory (WM) is crucial in everyday life; however, its neural mechanism has yet to be fully elucidated. Specifically, the role of the hippocampus, an essential brain region contributing to memory has been an ongoing topic [1] [2] [3] [4] [5] [6] [7] [8] [9]. Understanding the hippocampus' role in working memory is instrumental in deepening our knowledge of cognitive processes, ultimately aiding in developing cognitive training strategies and interventions.

It is known that a transient and synchronous oscillation called sharp-wave ripple (SWR) [10] is associated with various cognitive functions, including memory replay [11] [12] [13] [14] [15], memory consolidation [16] [17] [18] [19], memory recall [20] [21] [22], and neural plasticity [23] [24]. Thus, SWR might be a fundamental representation of processing in the hippocampus and contribute to working memory performances. However, investigations into the effects of SWRs on working memory remain infrequent ([25] and limited to rodent models using navigation tasks, in which precise timings of memory acquisition and recall are not separated.

Moreover, it is getting discovered that hippocampal neurons exhibit low-dimensional representations during

*Corresponding author. Tel: +81-6-6879-3652

WM tasks. For instance, the firing patterns of place cells [26] [27] [28] [29] [30] in the hippocampus were embedded within a dynamic, nonlinear three-dimensional hyperbolic geometry in rodent [31]. Furthermore, grid cells in the entorhinal cortex (EC) — the primary gateway to the hippocampus [32] [33] [34] — exhibited toroidal topology during exploration [35]. However, again, these experiments are limited to spatial navigation tasks in rodents so that the temporal resolution of WM tasks is constrained. Moreover, whther these findings are generalized to humans and beyond navigation tasks, are not investigated yet.

Given these backgrounds, in this study, we investigated the hypothesis that hippocampal neurons exhibit distinct representations in low-dimensional spaces as 'neural trajectory' during WM tasks, with a specific focus on SWR periods. To test this hypothesis, we utilized a dataset of patients performing an eight-second Sternberg task with high temporal resolution (1 s for fixation, 2 s for encoding, 3 s for maintenance, and 2 s for retrieval) while their intrachranial electroencephalography signals (iEEG) in the medial temporal lobe (MTL) were recorded [36]. To explore low-dimensional neural trajectories, we employed Gaussian-process factor analysis (GPFA) based on multiunit activities, a proven tool for the analysis of neural population dynamics [37].

2. Results

2.1. iEEG recording and neural trajectory in MTL regions during a Sternberg task

We employed a publicly available dataset [36] for this analysis. This dataset includes LFP signals (Figure 1A) within MTL regions (Table 1) during a modified Sternberg task. SWR^+ candidates were detected from LFP signals passed through the ripple band (80–140 Hz) (Figure 1B) within all hippocampal regions (refer to Methods), while SWR^- candidates were defined at identical timestamps of SWR^+ candidates but with shuffled across different trials (Figure 1). The multiunit spikes (Figure 1C) are included in the dataset as well, being established using a spike sorting algorithm [38]. Using the 50-ms binned multiunit activity without overlaps, we employed GPFA [37] to determine the neural trajectory (or factors) of the MTL regions by session and region (Figure 1D). Each factor was z-normalized by session and region (for example, session #2 in AHL of subject #1). The Euclidean distance from the origin (O) was calculated (Figure 1E).

2.2. Hippocampal neural trajectory correlated with a Sternberg task

In Figure 2A, the median neural trajectories of 50 trials were depicted as point clouds within the three major factor space. The optimal embedding dimension for the GPFA model was determined to be three using the elbow method (Figure 2B). The trajectory distance from the origin (O) ($\|g_F\|$, $\|g_E\|$, $\|g_M\|$, and $\|g_R\|$) of the hippocampus was larger than those of the EC and amygdala (Figure C & D).[1]

Similarly, the distance among geometric medians of the four phases were calculated: $\|g_F g_E\|$, $\|g_F g_M\|$, $\|g_F g_R\|$, $\|g_E g_M\|$, $\|g_E g_R\|$, and $\|g_M g_R\|$. Again, the hippocampus showed larger distances among phases compared to both the EC and amygdala. [2]

2.3. Memory load-dependent neural trajectory distance between the encoding and retrieval states in the hippocampus

Regarding the memory load of the Stenberg task, correct rate of trials and set size (= the number of alphabetical letters to encode) were negatively correlated (Figure 3A). [3] Similarly, response time and set size were positively correlated (Figure 3B).[4]

Furthermore, similarly, set size and the trajectory distance between the encoding and retrieval phases

[1] Hippocampus: Distance = 1.11 [1.01], median [IQR], n = 195,681 timepoints; EC: Distance = 0.94 [1.10], median [IQR], n = 133,761 timepoints; Amygdala: Distance = 0.78 [0.88], median [IQR], n = 165,281 timepoints.

[2] Hippocampus: Distance = 0.60 [0.70], median [IQR], n = 8,772 combinations; EC: Distance = 0.28 [0.52], median [IQR], n = 5,017 combinations ($p < 0.01$; Brunner–Munzel test); Amygdala: Distance = 0.24 [0.42], median [IQR], n = 7,466 combinations ($p < 0.01$; Brunner–Munzel test).

[3] Correct rate: set size four (0.99 ±0.11, mean ±SD; n = 333 trials) vs. set size six (0.93 ±0.26; n = 278 trials; $p < 0.001$, Brunner–Munzel test with Bonferroni correction) and set size eight (0.87 ±0.34; n = 275 trials; $p < 0.05$; Brunner–Munzel test with Bonferroni correction). Overall, $p < 0.001$ for Kruskal–Wallis test; correlation coefficient = -0.20, $p < 0.001$.

[4] Response time: set size four (1.26 ±0.45 s; n = 333 trials) vs. set size six (1.53 ±0.91 s; n = 278 trials) and set size eight (1.66 ±0.80 s; n = 275 trials). All comparisons $p < 0.001$, Brunner–Munzel test with Bonferroni correction; $p < 0.001$ for Kruskal–Wallis test; correlation coefficient = 0.22, $p < 0.001$

($\log_{10}\|g_E g_R\|$) were positively correlated (Figure 3C).[5], while distances between other phase combinations did not yield no significant correlations (Figures 3D & S2).

2.4. Detection of hippocampal SWR from putative CA1 regions

Under the aim to improve the precision of recording sites and the detection of SWRs, we estimated electrodes in CA1 regions of the hippocampus based on observing distinct multiunit spike patterns during SWR events. For each session and hippocampal region, SWR^+/SWR^- candidates were embedded into a two-dimensional space via UMAP (Figure 4A).[6] We calculated the silhouette score as a measure of clustering quality (Figure 4B & Table 2). Recording sites with an average silhouette score across sessions exceeding 0.6 were defined as putative CA1 regions [7] (Tables 2 & 3). Five putative CA1 regions were identified, and the four of them had not been labeled as seizure onset zones (Table 1).

Subsequently, SWR^+/SWR^- candidates within these putative CA1 regions were labeled SWR^+ and SWR^-, respectively[8] (Table 3). Both SWR^+ and SWR^- exhibited an identical duration[9] (Figure 4C) due to their definitions, following a log-distribution profile. A increase in SWR^+ incidence was detected during the initial 400 ms of the retrieval phase [10] (Figure 4D). Additionally, the peak ripple band amplitude of SWR^+ exceeded that of SWR^- and followed a log-normal distribution (Figure 4E).[11].

[5]Correlation between set size and $\log_{10}(\|g_E g_R\|)$: correlation coefficient = 0.05, $p < 0.001$. Specific values: $\|g_E g_R\|$ = 0.54 [0.70] for set size four trials, n = 447; $\|g_E g_R\|$ = 0.58 [0.66] for set size six trials, n = 381; $\|g_E g_R\|$ = 0.61 [0.63] for set size eight trials, n = 395.

[6]For illustrative purposes, consider the AHL in session #1 of subject #1.

[7]The identified regions were: AHL of subject #1, AHR of subject #3, PHL of subject #4, AHL of subject #6, and AHR of subject #9.

[8]Definitions lead to equal counts for both categories: SWR^+ (n = 1,170) and SWR^- (n = 1,170).

[9]Definitions lead to equal duration for both categories: SWR^+ (93.0 [65.4] ms) and SWR^- (93.0 [65.4] ms).

[10]SWR^+ increased against the bootstrap sample; 95th percentile = 0.42 [Hz]; $p < 0.05$.

[11]SWR^+ (3.05 [0.85] SD of baseline, median [IQR]; n = 1,170) vs. SWR^- (2.37 [0.33] SD of baseline, median [IQR]; n = 1,170; $p < 0.001$; Brunner–Munzel test).

2.5. Transient neural trajectory change in the hippocampus during SWR

The *distances* of trajectory from the origin (O) during SWR events in both the encoding and retrieval phases were calculated (Figure 5A). Given the distance increase during SWR as shown in Figure 5A, we categorized each SWR into three stages: pre-, mid-, and post-SWR. Subsequently, the distances from O during these SWR periods are represented as $\|\text{pre-eSWR}^+\|$, $\|\text{mid-eSWR}^+\|$, and so on.

$\|\text{mid-eSWR}^+\|$ [12] was larger than $\|\text{pre-eSWR}^+\|$ [13] , and $\|\text{mid-rSWR}^+\|$ [14] was larger than $\|\text{pre-rSWR}^+\|$ in both Match IN and Mismatch OUT tasks. [15]

2.6. Visualization of hippocampal neural trajectory during SWR in two-dimensional spaces

Based on our observations of neural trajectory 'jump' during SWR (Figure 5), we visualized the three-dimensional trajectories of pre-, mid-, and post-SWR events during the encoding and retrieval phases (Figure 6), the distance between which was memory-load dependent (Figure 3).

To achieve the visualization in two dimension spaces, peri-SWR trajectories were linearly aligned by positioning g_E at the origin (0, 0) and g_R at ($\|g_E g_R\|$, 0). These aligned trajectories were rotated around the $g_E g_R$ axis (= x-axis). Thus, distances from the origin O and angles between $g_E g_R$ in the original three-dimensional spaces are preserved in these two-dimensional ones.

The scatter plot in these two-dimensional spaces illustrates characteristic distributions of peri-SWR trajectories based on phases and task types. For instance, it is observable that $\|\text{mid-eSWR}^+\|$ is larger than $\|\text{pre-eSWR}^+\|$ (Figure 6B), consistent with our earlier findings (Figure 5).

2.7. Fluctuations of hippocampal neural trajectories between encoding and retrieval states

Subsequently, we checked trajectory *directions* based on $\overrightarrow{g_E g_R}$. SWR directions were defined by neural tra-

[12]1.25 [1.30], median [IQR], n = 1,281, in Match IN task; 1.12 [1.35], median [IQR], n = 1,163, in Mismatch OUT task

[13]1.08 [1.07], median [IQR], n = 1,149, in Match IN task; 0.90 [1.12], median [IQR], n = 1,088, in Mismatch OUT task

[14]1.32 [1.24], median [IQR], n = 935, in Match IN task; 1.15 [1.26], median [IQR], n = 891, in Mismatch OUT task

[15]1.19 [0.96], median [IQR], n = 673, in Match IN task; 0.94 [0.88], median [IQR], n = 664, in Mismatch OUT task

jectory at −250 ms and +250 ms from their center (*i.e.*, $\overrightarrow{\mathrm{eSWR}^{+}}$).

The density of $\overrightarrow{\mathrm{eSWR}} \cdot \overrightarrow{g_E g_R}$, $\overrightarrow{\mathrm{rSWR}} \cdot \overrightarrow{g_E g_R}$, and $\overrightarrow{\mathrm{eSWR}} \cdot \overrightarrow{\mathrm{rSWR}}$ were calculated (Figure 7A–D). $\overrightarrow{\mathrm{rSWR}^{-}} \cdot \overrightarrow{g_E g_R}$ showed biphasic distributions.

By taking the differences between the distribution of $\overrightarrow{\mathrm{rSWR}^{+}} \cdot \overrightarrow{g_E g_R}$ (Figure 7A & B) and those of $\overrightarrow{\mathrm{rSWR}^{-}} \cdot \overrightarrow{g_E g_R}$ (Figure 7C & D), the contributions of SWR was calculated (Figure 7E & F), revealing a shift in the direction of $\overrightarrow{g_E g_R}$ (Figure 7E & F; *red rectangles*).

Additionally, only in Mismatch OUT task, $\overrightarrow{\mathrm{eSWR}^{+}} \cdot \overrightarrow{\mathrm{rSWR}^{+}}$ was less than $\overrightarrow{\mathrm{eSWR}^{-}} \cdot \overrightarrow{\mathrm{rSWR}^{-}}$ (baseline periods) (Figure 7F; *pink circles*); in other words, eSWR and rSWR directed in the adverse direction solely in Mismatch OUT task but in Match IN task (Figure 7E; *pink circles*).

3. Discussion

This study hypothesized that hippocampal neurons exhibit distinct representations, or trajectories, in low-dimensional spaces during a WM task in humans, particularly during SWR periods. First, we projected the multiunit spikes in MTL regions during a Sternberg task onto three-dimensional spaces by GPFA (Figures 1D–E and Figure 2A). The distance of trajectory among WM phases ($\|g_F g_E\|$, $\|g_F g_M\|$, $\|g_F g_R\|$, $\|g_E g_M\|$, $\|g_E g_R\|$, and $\|g_M g_R\|$) was larger in the hippocampus than the EC and amygdala (Figure 2E), showing more dynamical neural activity in the hippocampus during the WM task. Additionally, the distance of trajectory between the encoding and retrieval phases in the hippocampus ($\|g_F g_E\|$) was positively correlated with memory load (Figures 3C & D), indicating it as a reflection of WM processing. Furthermore, the neural trajectory in the hippocampus showed transient increase during SWRs (Figure 5). Finally, the hippocampal neural trajectory fluctuated between encoding and retrieval states, with a shift from encoding to retrieval during SWR events (Figure 7). In sum, these results demonstrated the hippocampal neural behavior in a WM task in humans.

First, we found that the distance of the neural trajectory among the four phases ($\|g_F g_E\|$, $\|g_F g_M\|$, $\|g_F g_R\|$, $\|g_E g_M\|$, $\|g_E g_R\|$, and $\|g_M g_R\|$) was longer in the hippocampus compared to the EC and amygdala, even considering the distance from O ($\|g_F\|$, $\|g_E\|$, $\|g_M\|$, and $\|g_R\|$) in those regions (Figures 2C–E). These results indicate hippocampal participation in the WM task, which is partially supported by previous findings of hippocampal persistent firing in the maintenance phase [3] [4] [5] [6]. However, by applying GPFA to multiunit activity during the 1-s level resolution of WM task, we revealed that the neural trajectory in low dimensional space displayed memory-load dependency between the encoding and retrieval phase, represented as $\|g_E g_R\|$ (Figure 3). Overall, these results provide evidence that the hippocampus is linked to WM processing.

The validity of our analysis of confining to putative CA1 regions (Figure 4) is supported by several factors. First, this targeted approach stems from well-established observations that SWRs are time-locked to synchronous spike bursts of interneurons and pyramidal neurons [39] [40] [41] [42], potentially around 50 μm radius of the recording site [43]. Additionally, in the present study, we found the increase in SWRs' incidence at 0–400 ms of the retrieval phase (Figure 4D). This result is consistent with previous reports showing increased SWR occurrence before spontaneous verbal recall [21] [22]. Thus, our result is not only consistent but also extends the finding to a triggered retrieval condition. Moreover, the log-normal distributions of SWR duration and ripple band peak amplitude observed in this study (Figure 4C & E) align with the consensus in this field [44]. Therefore, our approach of limiting recording sites for putative CA1 regions would have contributed to precision of SWR detection. One limitation is that the increase in trajectory distance from O during SWR (Figure 5) would have been biased to greater due to the channel selection; however, this is not critical for our major findings.

Interestingly, the trajectory directions in the retrieval phase oscillated between the encoding and retrieval states both in baseline and SWR periods (Figures 7C & D). In addition, the balance of such fluctuation was shifted from the encoding to retrieval state during SWR (Figures 7 E & F). These results are again consistent with previous reports suggesting SWR's role in memory recall [21] [22]. Our result adds another layer of understanding, that is, SWR occurs when hippocampal representation proceeds "from encoding" to retrieval states. Therefore, our results provide new aspects of hippocampal representations: (i) neural fluctuations between encoding and retrieval states during a WM task and (ii)

SWR as a switching representation from encoding to retrieval states.

Moreover, our study reveals WM-task type specific directions between encoding- and retrieval-SWRs (Figure 7E–F). Specifically, eSWR and rSWR directed in the adverse direction not in Match IN but in Mismatch OUT task. These result might be explained by the memory engram theory [45]. In fact, Match In task exposed subjects to once-seen letter, while Mismatch OUT task a novel letter which was not included in the encoding phase. These results suggest that SWR is related to working cognitive processess in humans.

In conclusion, our study has demonstrated that hippocampal activity fluctuates between encoding and retrieval states during a WM task and exhibits a significant transition "from encoding" to retrieval during SWR periods.

References

[1] W. B. Scoville, B. Milner, LOSS OF RECENT MEMORY AFTER BILATERAL HIPPOCAMPAL LESIONS, Journal of Neurology, Neurosurgery, and Psychiatry 20 (1) (1957) 11–21.
URL https://www.ncbi.nlm.nih.gov/pmc/articles/PMC497229/

[2] L. R. Squire, The Legacy of Patient H.M. for Neuroscience, Neuron 61 (1) (2009) 6–9. doi:10.1016/j.neuron.2008.12.023.
URL https://www.ncbi.nlm.nih.gov/pmc/articles/PMC2649674/

[3] E. Boran, T. Fedele, P. Klaver, P. Hilfiker, L. Stieglitz, T. Grunwald, J. Sarnthein, Persistent hippocampal neural firing and hippocampal-cortical coupling predict verbal working memory load, Science Advances 5 (3) (2019) eaav3687. doi:10.1126/sciadv.aav3687.
URL https://www.science.org/doi/10.1126/sciadv.aav3687

[4] J. Kamiński, S. Sullivan, J. M. Chung, I. B. Ross, A. N. Mamelak, U. Rutishauser, Persistently active neurons in human medial frontal and medial temporal lobe support working memory, Nature Neuroscience 20 (4) (2017) 590–601, number: 4 Publisher: Nature Publishing Group. doi:10.1038/nn.4509.
URL https://www.nature.com/articles/nn.4509

[5] S. Kornblith, R. Q. Quiroga, C. Koch, I. Fried, F. Mormann, Persistent Single-Neuron Activity during Working Memory in the Human Medial Temporal Lobe, Current Biology 27 (7) (2017) 1026–1032, publisher: Elsevier. doi:10.1016/j.cub.2017.02.013.
URL https://www.cell.com/current-biology/abstract/S0960-9822(17)30149-5

[6] M. C. M. Faraut, A. A. Carlson, S. Sullivan, O. Tudusciuc, I. Ross, C. M. Reed, J. M. Chung, A. N. Mamelak, U. Rutishauser, Dataset of human medial temporal lobe single neuron activity during declarative memory encoding and recognition, Scientific Data 5 (1) (2018) 180010, number: 1 Publisher: Nature Publishing Group. doi:10.1038/sdata.2018.10.
URL https://www.nature.com/articles/sdata201810

[7] A. A. Borders, C. Ranganath, A. P. Yonelinas, The hippocampus supports high-precision binding in visual working memory, Hippocampus 32 (3) (2022) 217–230. doi:10.1002/hipo.23401.

[8] J. Li, D. Cao, S. Yu, X. Xiao, L. Imbach, L. Stieglitz, J. Sarnthein, T. Jiang, Functional specialization and interaction in the amygdala-hippocampus circuit during working memory processing, Nature Communications 14 (1) (2023) 2921, number: 1 Publisher: Nature Publishing Group. doi:10.1038/s41467-023-38571-w.
URL https://www.nature.com/articles/s41467-023-38571-w

[9] V. Dimakopoulos, P. Mégevand, L. H. Stieglitz, L. Imbach, J. Sarnthein, Information flows from hippocampus to auditory cortex during replay of verbal working memory items, eLife 11 (2022) e78677, publisher: eLife Sciences Publications, Ltd. doi:10.7554/eLife.78677.
URL https://doi.org/10.7554/eLife.78677

[10] G. Buzsáki, Hippocampal sharp wave-ripple: A cognitive biomarker for episodic memory and planning, Hippocampus 25 (10) (2015) 1073–1188, _eprint: https://onlinelibrary.wiley.com/doi/pdf/10.1002/hipo.22488. doi:https://doi.org/10.1002/hipo.22488.
URL https://onlinelibrary.wiley.com/doi/abs/10.1002/hipo.22488

[11] M. A. Wilson, B. L. McNaughton, Reactivation of hippocampal ensemble memories during sleep, Science (New York, N.Y.) 265 (5172) (1994) 676–679. doi:10.1126/science.8036517.

[12] Z. Nádasdy, H. Hirase, A. Czurkó, J. Csicsvari, G. Buzsáki, Replay and Time Compression of Recurring Spike Sequences in the Hippocampus, Journal of Neuroscience 19 (21) (1999) 9497–9507, publisher: Society for Neuroscience Section: ARTICLE. doi:10.1523/JNEUROSCI.19-21-09497.1999.
URL https://www.jneurosci.org/content/19/21/9497

[13] A. K. Lee, M. A. Wilson, Memory of sequential experience in the hippocampus during slow wave sleep, Neuron 36 (6) (2002) 1183–1194. doi:10.1016/s0896-6273(02)01096-6.

[14] K. Diba, G. Buzsáki, Forward and reverse hippocampal place-cell sequences during ripples, Nature Neuroscience 10 (10) (2007) 1241–1242, number: 10 Publisher: Nature Publishing Group. doi:10.1038/nn1961.
URL https://www.nature.com/articles/nn1961

[15] T. J. Davidson, F. Kloosterman, M. A. Wilson, Hippocampal replay of extended experience, Neuron 63 (4) (2009) 497–507. doi:10.1016/j.neuron.2009.07.027.

[16] G. Girardeau, K. Benchenane, S. I. Wiener, G. Buzsáki, M. B. Zugaro, Selective suppression of hippocampal ripples impairs spatial memory, Nature Neuroscience 12 (10) (2009) 1222–1223. doi:10.1038/nn.2384.
URL http://www.nature.com/articles/nn.2384

[17] V. Ego-Stengel, M. A. Wilson, Disruption of ripple-associated hippocampal activity during rest impairs spatial learning in the rat, Hippocampus 20 (1) (2010) 1–10. doi:10.1002/hipo.

20707.

[18] A. Fernández-Ruiz, A. Oliva, E. Fermino de Oliveira, F. Rocha-Almeida, D. Tingley, G. Buzsáki, Long-duration hippocampal sharp wave ripples improve memory, Science (New York, N.Y.) 364 (6445) (2019) 1082–1086. doi:10.1126/science.aax0758.
URL https://www.ncbi.nlm.nih.gov/pmc/articles/PMC6693581/

[19] J. Kim, A. Joshi, L. Frank, K. Ganguly, Cortical–hippocampal coupling during manifold exploration in motor cortex, Nature (2022) 1–8Publisher: Nature Publishing Group. doi:10.1038/s41586-022-05533-z.
URL https://www.nature.com/articles/s41586-022-05533-z

[20] C.-T. Wu, D. Haggerty, C. Kemere, D. Ji, Hippocampal awake replay in fear memory retrieval, Nature Neuroscience 20 (4) (2017) 571–580. doi:10.1038/nn.4507.

[21] Y. Norman, E. M. Yeagle, S. Khuvis, M. Harel, A. D. Mehta, R. Malach, Hippocampal sharp-wave ripples linked to visual episodic recollection in humans, Science 365 (6454) (2019) eaax1030. doi:10.1126/science.aax1030.
URL https://www.sciencemag.org/lookup/doi/10.1126/science.aax1030

[22] Y. Norman, O. Raccah, S. Liu, J. Parvizi, R. Malach, Hippocampal ripples and their coordinated dialogue with the default mode network during recent and remote recollection, Neuron 109 (17) (2021) 2767–2780.e5, publisher: Elsevier. doi:10.1016/j.neuron.2021.06.020.
URL https://www.cell.com/neuron/abstract/S0896-6273(21)00461-X

[23] C. J. Behrens, L. P. van den Boom, L. de Hoz, A. Friedman, U. Heinemann, Induction of sharp wave–ripple complexes in vitro and reorganization of hippocampal networks, Nature Neuroscience 8 (11) (2005) 1560–1567, number: 11 Publisher: Nature Publishing Group. doi:10.1038/nn1571.
URL https://www.nature.com/articles/nn1571

[24] H. Norimoto, K. Makino, M. Gao, Y. Shikano, K. Okamoto, T. Ishikawa, T. Sasaki, H. Hioki, S. Fujisawa, Y. Ikegaya, Hippocampal ripples down-regulate synapses, Science (New York, N.Y.) 359 (6383) (2018) 1524–1527. doi:10.1126/science.aao0702.

[25] S. P. Jadhav, C. Kemere, P. W. German, L. M. Frank, Awake Hippocampal Sharp-Wave Ripples Support Spatial Memory, Science 336 (6087) (2012) 1454–1458, publisher: American Association for the Advancement of Science. doi:10.1126/science.1217230.
URL https://www.science.org/doi/abs/10.1126/science.1217230

[26] J. O'Keefe, J. Dostrovsky, The hippocampus as a spatial map: Preliminary evidence from unit activity in the freely-moving rat, Brain Research 34 (1971) 171–175, place: Netherlands Publisher: Elsevier Science. doi:10.1016/0006-8993(71)90358-1.

[27] J. O'Keefe, Place units in the hippocampus of the freely moving rat, Experimental Neurology 51 (1) (1976) 78–109. doi:10.1016/0014-4886(76)90055-8.
URL https://www.sciencedirect.com/science/article/pii/0014488676900558

[28] A. D. Ekstrom, M. J. Kahana, J. B. Caplan, T. A. Fields, E. A. Isham, E. L. Newman, I. Fried, Cellular networks underlying human spatial navigation, Nature 425 (6954) (2003) 184–188, number: 6954 Publisher: Nature Publishing Group. doi:10.1038/nature01964.
URL https://www.nature.com/articles/nature01964

[29] K. B. Kjelstrup, T. Solstad, V. H. Brun, T. Hafting, S. Leutgeb, M. P. Witter, E. I. Moser, M.-B. Moser, Finite Scale of Spatial Representation in the Hippocampus, Science 321 (5885) (2008) 140–143, publisher: American Association for the Advancement of Science. doi:10.1126/science.1157086.
URL https://www.science.org/doi/abs/10.1126/science.1157086

[30] C. D. Harvey, F. Collman, D. A. Dombeck, D. W. Tank, Intracellular dynamics of hippocampal place cells during virtual navigation, Nature 461 (7266) (2009) 941–946, number: 7266 Publisher: Nature Publishing Group. doi:10.1038/nature08499.
URL https://www.nature.com/articles/nature08499

[31] H. Zhang, P. D. Rich, A. K. Lee, T. O. Sharpee, Hippocampal spatial representations exhibit a hyperbolic geometry that expands with experience, Nature Neuroscience (Dec. 2022). doi:10.1038/s41593-022-01212-4.
URL https://www.nature.com/articles/s41593-022-01212-4

[32] P. A. Naber, F. H. Lopes da Silva, M. P. Witter, Reciprocal connections between the entorhinal cortex and hippocampal fields CA1 and the subiculum are in register with the projections from CA1 to the subiculum, Hippocampus 11 (2) (2001) 99–104, _eprint: https://onlinelibrary.wiley.com/doi/pdf/10.1002/hipo.1028. doi:10.1002/hipo.1028.
URL https://onlinelibrary.wiley.com/doi/abs/10.1002/hipo.1028

[33] N. M. van Strien, N. L. M. Cappaert, M. P. Witter, The anatomy of memory: an interactive overview of the parahippocampal–hippocampal network, Nature Reviews Neuroscience 10 (4) (2009) 272–282, number: 4 Publisher: Nature Publishing Group. doi:10.1038/nrn2614.
URL https://www.nature.com/articles/nrn2614

[34] B. A. Strange, M. P. Witter, E. S. Lein, E. I. Moser, Functional organization of the hippocampal longitudinal axis, Nature Reviews Neuroscience 15 (10) (2014) 655–669, number: 10 Publisher: Nature Publishing Group. doi:10.1038/nrn3785.
URL https://www.nature.com/articles/nrn3785

[35] R. J. Gardner, E. Hermansen, M. Pachitariu, Y. Burak, N. A. Baas, B. A. Dunn, M.-B. Moser, E. I. Moser, Toroidal topology of population activity in grid cells, Nature 602 (7895) (2022) 123–128, number: 7895 Publisher: Nature Publishing Group. doi:10.1038/s41586-021-04268-7.
URL https://www.nature.com/articles/s41586-021-04268-7

[36] E. Boran, T. Fedele, A. Steiner, P. Hilfiker, L. Stieglitz, T. Grunwald, J. Sarnthein, Dataset of human medial temporal lobe neurons, scalp and intracranial EEG during a verbal working memory task, Scientific Data 7 (1) (2020) 30, number: 1 Publisher: Nature Publishing Group. doi:10.1038/s41597-020-0364-3.
URL https://www.nature.com/articles/s41597-020-0364-3

[37] B. M. Yu, J. P. Cunningham, G. Santhanam, S. I. Ryu, K. V. Shenoy, M. Sahani, Gaussian-Process Factor Analysis for Low-Dimensional Single-Trial Analysis of Neural Population Activity, Journal of Neurophysiology 102 (1) (2009) 614–635. doi:10.1152/jn.90941.2008.
URL https://www.ncbi.nlm.nih.gov/pmc/articles/PMC2712272/

[38] J. Niediek, J. Boström, C. E. Elger, F. Mormann, Reliable Analysis of Single-Unit Recordings from the Human Brain under Noisy Conditions: Tracking Neurons over Hours, PLOS ONE 11 (12) (2016) e0166598, publisher: Public Library of Science. doi:10.1371/journal.pone.0166598.
URL https://journals.plos.org/plosone/article?id=10.1371/journal.pone.0166598

[39] G. Buzsáki, Two-stage model of memory trace formation: a role for "noisy" brain states, Neuroscience 31 (3) (1989) 551–570. doi:10.1016/0306-4522(89)90423-5.

[40] M. L. V. Quyen, A. Bragin, R. Staba, B. Crépon, C. L. Wilson, J. Engel, Cell Type-Specific Firing during Ripple Oscillations in the Hippocampal Formation of Humans, Journal of Neuroscience 28 (24) (2008) 6104–6110, publisher: Society for Neuroscience Section: Brief Communications. doi:10.1523/JNEUROSCI.0437-08.2008.
URL https://www.jneurosci.org/content/28/24/6104

[41] S. Royer, B. V. Zemelman, A. Losonczy, J. Kim, F. Chance, J. C. Magee, G. Buzsáki, Control of timing, rate and bursts of hippocampal place cells by dendritic and somatic inhibition, Nature Neuroscience 15 (5) (2012) 769–775, number: 5 Publisher: Nature Publishing Group. doi:10.1038/nn.3077.
URL https://www.nature.com/articles/nn.3077

[42] N. Hájos, M. R. Karlócai, B. Németh, I. Ulbert, H. Monyer, G. Szabó, F. Erdélyi, T. F. Freund, A. I. Gulyás, Input-output features of anatomically identified CA3 neurons during hippocampal sharp wave/ripple oscillation in vitro, The Journal of Neuroscience: The Official Journal of the Society for Neuroscience 33 (28) (2013) 11677–11691. doi:10.1523/JNEUROSCI.5729-12.2013.

[43] E. W. Schomburg, C. A. Anastassiou, G. Buzsáki, C. Koch, The Spiking Component of Oscillatory Extracellular Potentials in the Rat Hippocampus, The Journal of Neuroscience 32 (34) (2012) 11798–11811. doi:10.1523/JNEUROSCI.0656-12.2012.
URL https://www.ncbi.nlm.nih.gov/pmc/articles/PMC3459239/

[44] A. A. Liu, S. Henin, S. Abbaspoor, A. Bragin, E. A. Buffalo, J. S. Farrell, D. J. Foster, L. M. Frank, T. Gedankien, J. Gotman, J. A. Guidera, K. L. Hoffman, J. Jacobs, M. J. Kahana, L. Li, Z. Liao, J. J. Lin, A. Losonczy, R. Malach, M. A. van der Meer, K. McClain, B. L. McNaughton, Y. Norman, A. Navas-Olive, L. M. de la Prida, J. W. Rueckemann, J. J. Sakon, I. Skelin, I. Soltesz, B. P. Staresina, S. A. Weiss, M. A. Wilson, K. A. Zaghloul, M. Zugaro, G. Buzsáki, A consensus statement on detection of hippocampal sharp wave ripples and differentiation from other fast oscillations, Nature Communications 13 (1) (2022) 6000, number: 1 Publisher: Nature Publishing Group. doi:10.1038/s41467-022-33536-x.
URL https://www.nature.com/articles/s41467-022-33536-x

[45] X. Liu, S. Ramirez, P. T. Pang, C. B. Puryear, A. Govindarajan, K. Deisseroth, S. Tonegawa, Optogenetic stimulation of a hippocampal engram activates fear memory recall, Nature 484 (7394) (2012) 381–385, number: 7394 Publisher: Nature Publishing Group. doi:10.1038/nature11028.
URL https://www.nature.com/articles/nature11028

[46] L. McInnes, J. Healy, N. Saul, L. Großberger, UMAP: Uniform Manifold Approximation and Projection, Journal of Open Source Software 3 (29) (2018) 861. doi:10.21105/joss.00861.
URL https://joss.theoj.org/papers/10.21105/joss.00861

Contributors

Y.W. and T.Y. conceptualized the study; Y.W. performed the data analysis; Y.W. and T.Y. wrote the original draft; and all authors reviewed the final manuscript.

Acknowledgments

This research was funded by a grant from the Exploratory Research for Advanced Technology (JPMJER1801).

Declaration of Interests

The authors declare that they have no competing interests.

Data and code availability

The data is available on G-Node (https://doi.gin.g-node.org/10.12751/g-node.d76994/).
The source code is available on GitHub (https://github.com/yanagisawa-lab/hippocampal-neural-fluctuation-during-a-WM-task-in-hum

Inclusion and Diversity Statement

We support inclusive, diverse, and equitable conduct of research.

Declaration of Generative AI in Scientific Writing

The authors employed ChatGPT, provided by OpenAI, for enhancing the manuscript's English language quality. After incorporating the suggested improvements, the authors meticulously revised the content. Ultimate responsibility for the final content of this publication rests entirely with the authors.

Figures

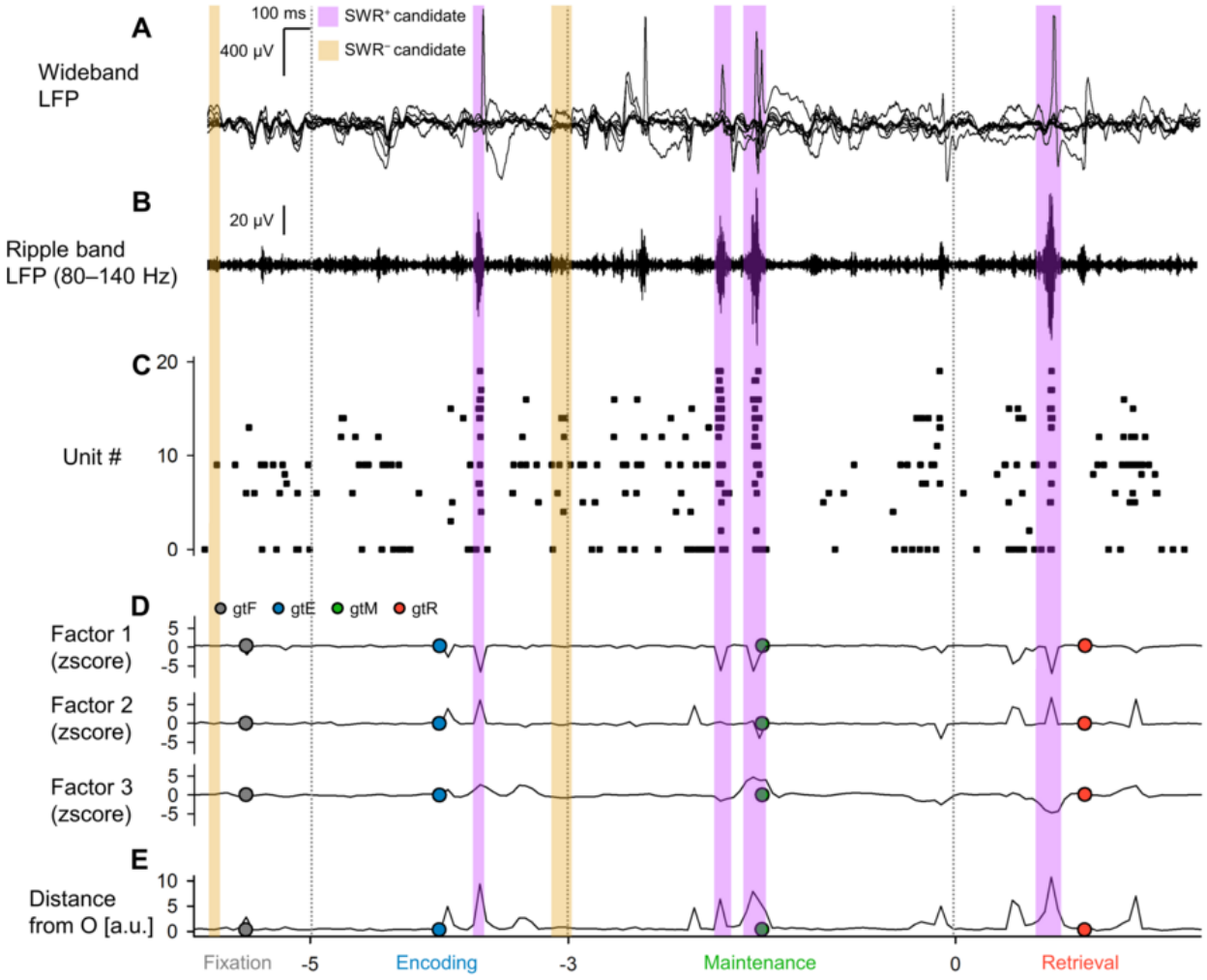

Figure 1 – Local field potential (LFP), multiunit activity, and neural trajectory of the hippocampus during a modified Sternberg task

A. Representative wideband LFP traces iEEG signals recorded in the left hippocampal head. The subject conducted a modified Sternberg working memory task, including fixation (1 s, *gray*), encoding (2 s, *blue*), maintenance (3 s, *green*), and retrieval (2 s, *red*). ***B.*** The corresponding ripple band LFP traces. ***C.*** The raster plot of multiunit spikes estimated from the LFP traces using a spike sorting algorithm [38]. ***D.*** Neural trajectory calculated by GPFA on spike counts per unit with 50-ms bins. The dot circles show the coordinate of geometric median for each phase. ***E.*** Trajectory distance from the origin *O*. Note that *purple* and *yellow* rectangles shows the timings for SWR^{+} candidates and SWR^{-} candidates (control for SWR^{+}), respectively.

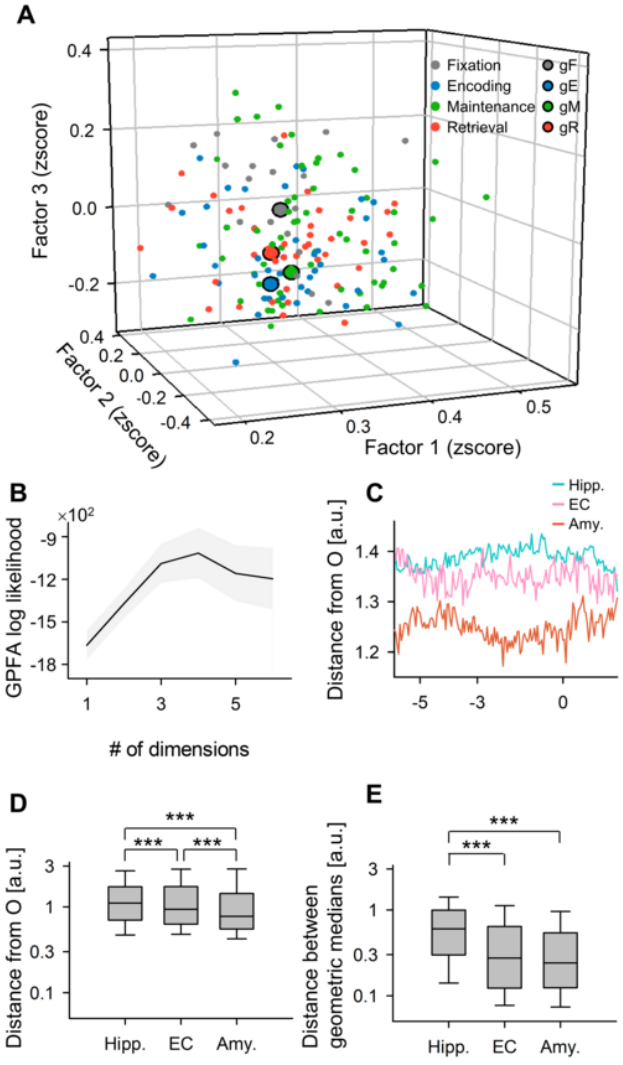

Figure 2 – State-dependent hippocampal neural trajectory

A. Neural trajectory in the first three-dimensional factors calculated by GPFA. Smaller dots indicate coordinates of 50-ms neural trajectory bins. Larger dots with *black* edges represent geometric medians for the following phases in the Sternberg working memory task: fixation (*gray*), encoding (*blue*), maintenance (*green*), and retrieval (*red*). ***B.*** The log-likelihood of GPFA models in relation to the number of dimensions to embed multiunit spikes in MTL regions. Notably, the optimal dimension was identified as three using the elbow method. ***C.*** Distance of neural trajectory from the origin (*O*) for the hippocampus (Hipp.), entorhinal cortex (EC), and amygdala (Amy.), plotted against the time from probe onset. ***D.*** Trajectory distance from *O* in MTL regions, with the hippocampus showing the greatest distance, followed by the EC and the Amygdala. ***E.*** Inter-phase trajectory distances in the MTL regions. Abbreviations:

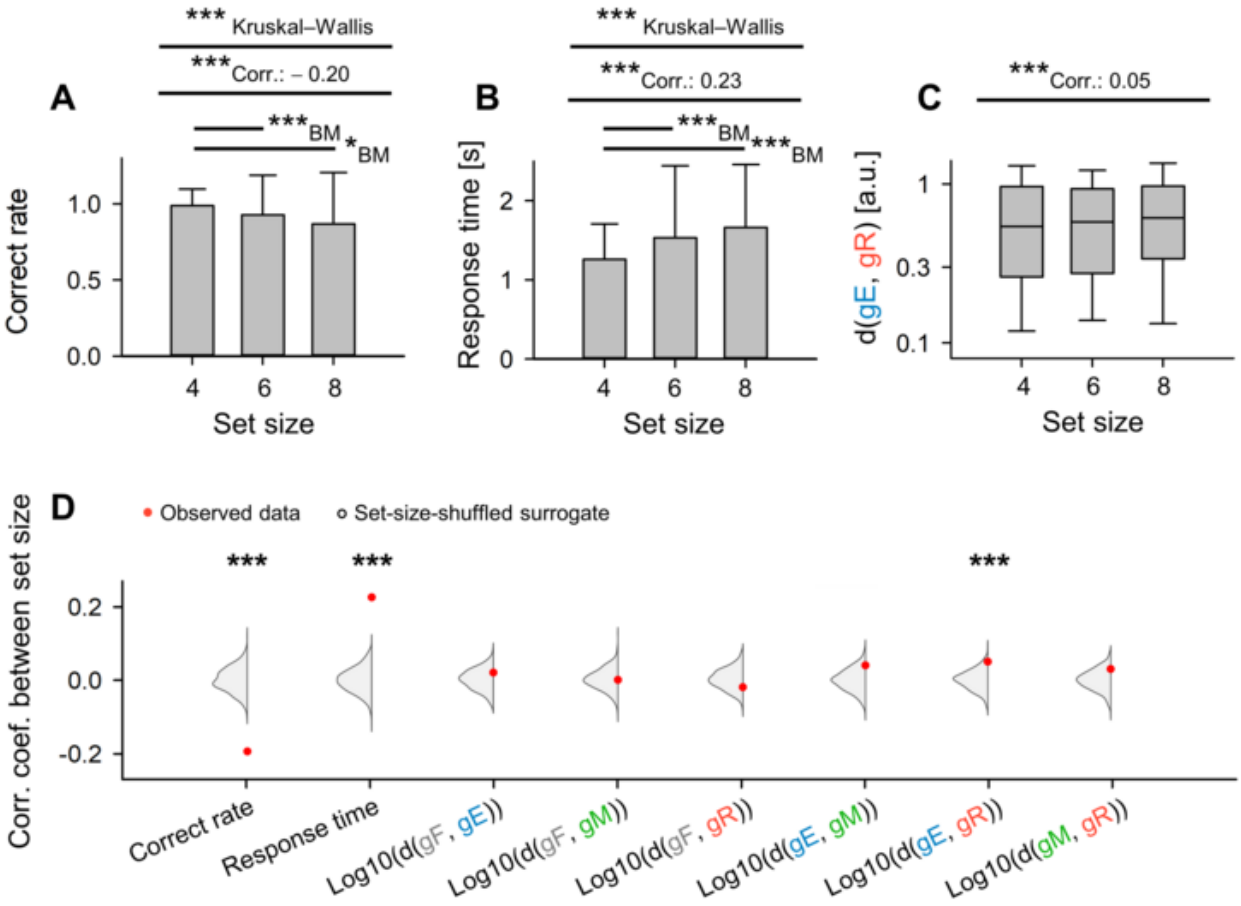

Figure 3 – Memory-load dependency in trajectory distance between encoding and retrieval states in the hippocampus

A. Set size (number of letters to encode) and correct rate in the WM task (coefficient = −0.20, ***$p < 0.001$). ***B.*** Set size and response time (coefficient = 0.23, ***$p < 0.001$). ***C.*** Set size and the inter-phase distances between encoding and retrieval phases ($\|g_E g_R\|$) (correlation coefficient = 0.05). ***D.*** *Red* dots show experimentally observed correlations between set size and the following parameters: correct rate, response time, $\log_{10}\|g_F g_E\|$, $\log_{10}\|g_F g_M\|$, $\log_{10}\|g_F g_R\|$, $\log_{10}\|g_E g_M\|$, $\log_{10}\|g_E g_R\|$, and $\log_{10}\|g_M g_R\|$. The *gray* kernel density plot shows corresponding set-size-shuffled surrogate (n = 1,000) (***ps < 0.001).

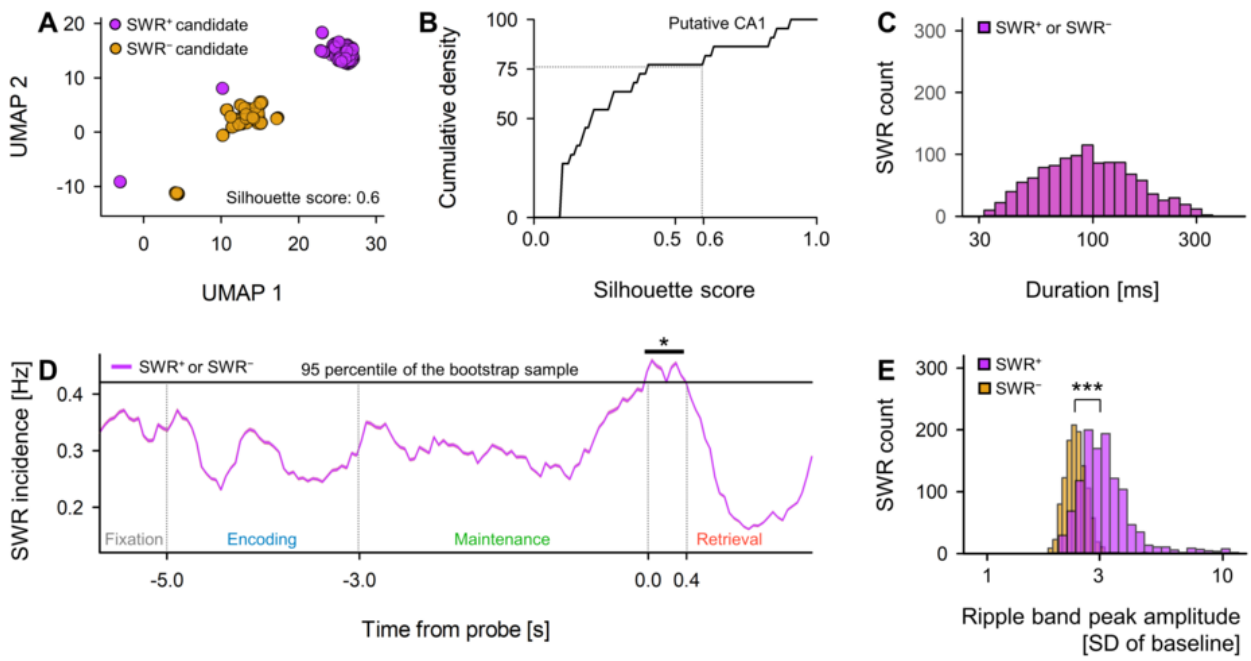

Figure 4 – SWR detection in putative CA1 regions

A. Two-dimensional UMAP (uniform manifold approximation and projection)[46] projection of multiunit spikes during SWR$^+$ candidates (*purple*) and SWR$^-$ candidates (*yellow*). ***B.*** Cumulative density plot of silhouette scores, a barometer for UMAP clustering quality, for hippocampal regions (refer to Table 2). Note that hippocampal regions with silhouette scores exceeding 0.60 (= 75th percentile) were defined as putative CA1 regions. SWR$^+$ and SWR$^-$ candidates recorded in these putative CA1 regions were defined as SWR$^+$ and SWR$^-$ (*n*s = 1,170), respectively. ***C.*** The distributions of durations for SWR$^+$ (*purple*) and SWR$^-$ (*yellow*), which are identical due to their definitions (93.0 [65.4] ms, median [IQR]). ***D.*** SWR incidence for both SWR$^+$ (*purple*) and SWR$^-$ (*yellow*) relative to time from probe, represented as mean ±95% confidence interval, although the intervals might not be visible due to their narrow range. Note the significant elevation in SWR incidence was detected during the first 400 ms of the retrieval phase (0.421 [Hz], $*p < 0.05$, bootstrap test). ***E.*** The distributions of ripple band peak amplitude for SWR$^-$ (*yellow*; 2.37 [0.33] SD of baseline, median [IQR]) and SWR$^+$ (*purple*; 3.05 [0.85] SD of baseline, median [IQR]) ($***p < 0.001$, the Brunner–Munzel test).

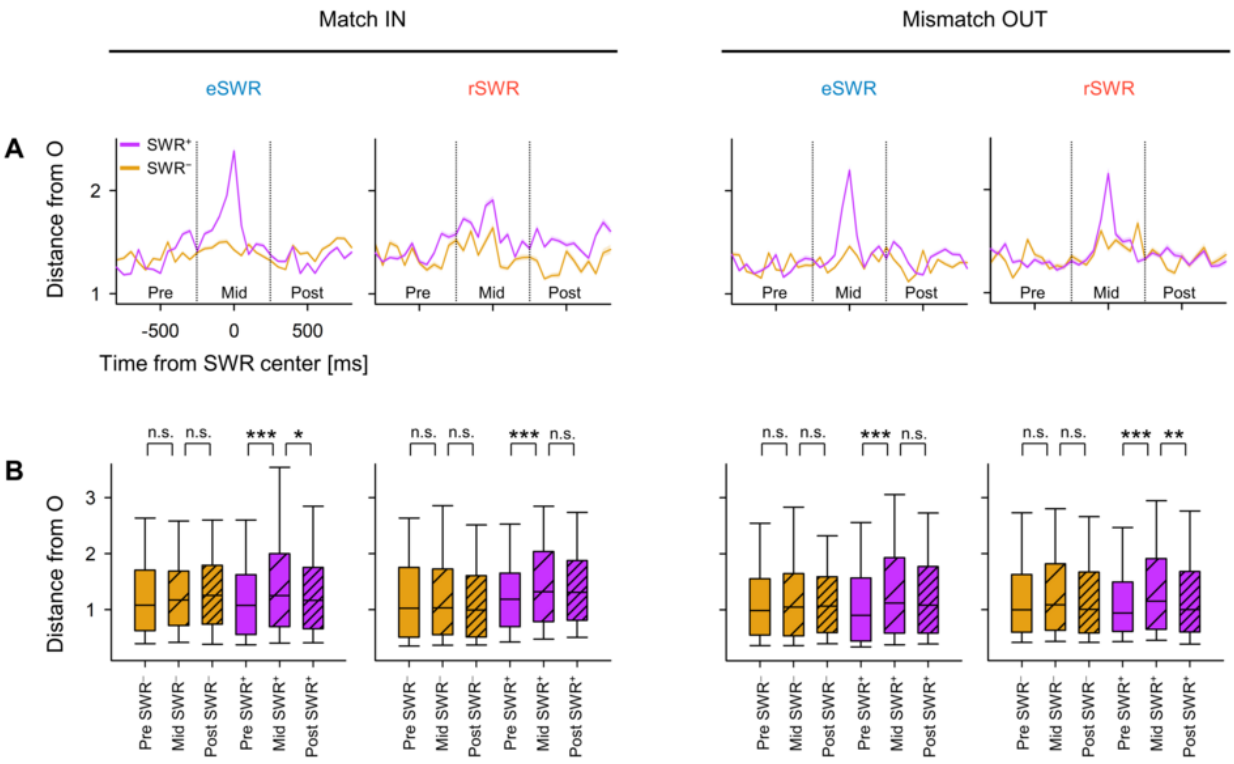

Figure 5 – Transient neural trajectory change during SWR

A. Distance from the origin (O) of the peri-sharp-wave-ripple trajectory (mean ±95% confidence interval, although the intervals might not be visible due to their narrow ranges. ***B.*** The distance from the origin (O) during pre-, mid-, and post-SWR periods (*$p < 0.05$, **$p < 0.01$, ***$p < 0.001$; Brunner–Munzel test). Abbreviations: SWR, sharp-wave ripple events; eSWR, SWR during the encoding phase; rSWR, SWR during the retrieval phase, SWR^+, SWR event; SWR^- control events for SWR^+; pre-, mid-, or post-SWR, the time interval from −800 to −250 ms, from −250 to +250 ms, or from +250 to +800 ms relative to SWR center.

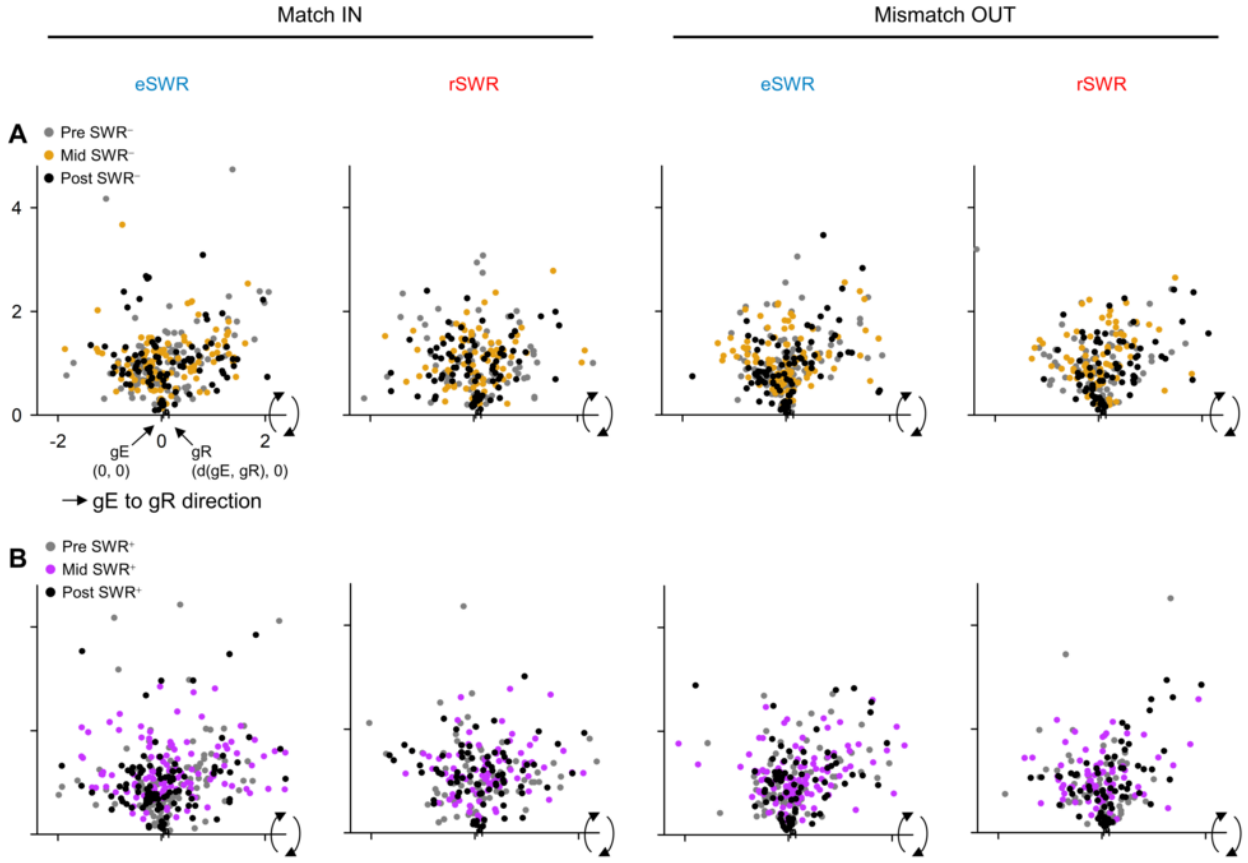

Figure 6 – Coordinates of neural trajectory during sharp-wave ripple aligned by encoding and retrieval states.

A. Hippocampal neural trajectories during pre- (*gray*), mid- (*yellow*), and post-SWR$^-$ (*black*) in Match IN (*left*) and Mismatch OUT task (*right*). ***B.*** The equivalents for SWR$^+$ instead of SWR$^-$, though mid-SWR$^+$ is depicted with *purple*. All data points underwent adjustments and rotations to fit a two-dimensional representation, positioning g_E at (0, 0) and g_R at ($\|g_E g_R\|$, 0). The $\|g_E g_R\|$ metric varies across sessions, and its median ±IQR (with medians approximately 0.2) is presented on the x-axes. Note: some intervals might be challenging to discern because of their narrow range. In this two-dimensional depiction, both the distances and angles preserve their relationships as in the original three-dimensional space. Abbreviations: SWR, sharp-wave ripple events; eSWR, SWR during the encoding phase; rSWR, SWR during the retrieval phase, SWR$^+$, SWR event; SWR$^-$ control events for SWR$^+$; pre-SWR, mid-SWR, or post-SWR, the time interval from −800 to −250 ms, from −250 to +250 ms, or from +250 to +800 ms from the center of SWR.

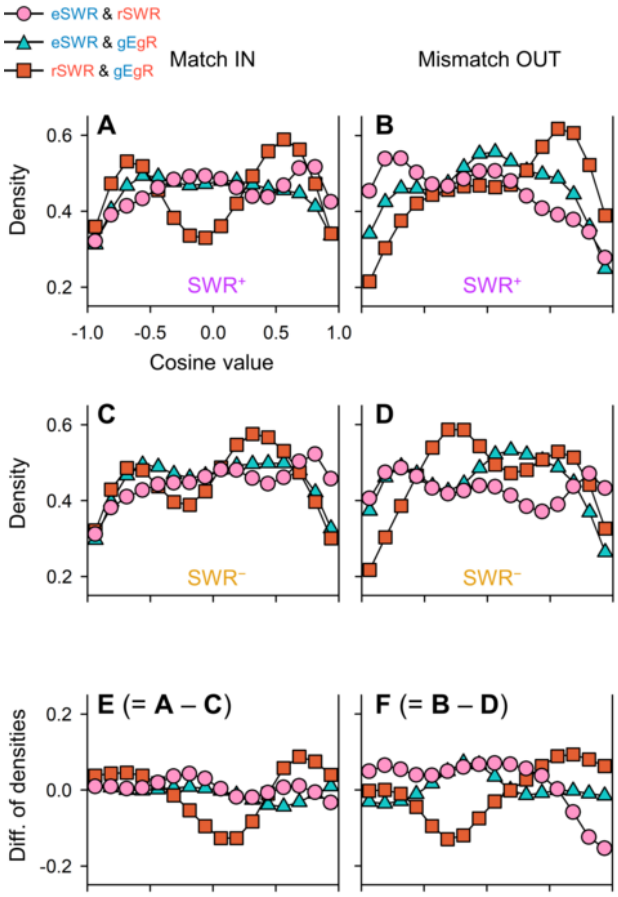

Figure 7 – Analysis of Neural Trajectory Directions during SWR between Encoding, and Retrieval States.

A–B Kernel density estimation (KDE) distribution of $\overrightarrow{\mathrm{eSWR}^+} \cdot \overrightarrow{\mathrm{rSWR}^+}$ (*pink circles*), $\overrightarrow{\mathrm{eSWR}^+} \cdot \overrightarrow{\mathrm{g_E g_R}}$ (*blue triangles*), and $\overrightarrow{\mathrm{rSWR}^+} \cdot \overrightarrow{\mathrm{g_E g_R}}$ (*red rectangles*) in Match In (***A***) and Mismatch OUT task (***B***). ***C–D.*** The corresponding distributions of SWR^- in response to those of SWR^+ in ***A–B***. ***E–F.*** The differences in distributions, highlighting the SWR components (***E*** = ***C*** − ***A***; ***F*** = ***B*** − ***D***). Note the inverse directionality between $\overrightarrow{\mathrm{eSWR}^+}$ and $\overrightarrow{\mathrm{rSWR}^+}$ only in Mismatch OUT task (*pink circles* in ***E–F***). Additionally, the shifts from the retrieval to encoding states were observed for SWR components both in Match IN and Mismatch OUT tasks (*red rectangles* in ***E–F***).